APP Template V1.52 Article id: sst500008 Typesetter: MPS Date received by MPS: 08/08/2014 PE: MAC003297 CE: LE:



IOP Publishing Semiconductor Science and Technology

Semicond. Sci. Technol. **00** (2014) 000000 (7pp)

# Localization and field-periodic conductance fluctuations in trilayer graphene

**Mohammed S El-Bana[1,2], Daniel Wolverson[1], David W Horsell[3] and Simon J Bending[1]**

[1] Department of Physics, University of Bath, Claverton Down, Bath BA2 7AY, UK
[2] Department of Physics, Faculty of Education, Ain Shams University, Cairo, Egypt
[3] School of Physics, University of Exeter, Exeter EX4 4QL, UK

Received 17 June 2014, revised 22 July 2014
Accepted for publication 29 July 2014
Published DD MM 2014

**Abstract**

Q1 We have systematically studied quantum transport in a short (of the same order of magnitude as the carrier phase-breaking length) trilayer-graphene field-effect transistor. Close to the charge neutrality point, our magnetoconductance data are well described by the theory of weak localization in monolayer graphene. However, as the carrier density is increased we find a complex evolution of the low field magnetoconductance that originates from a combination of the monolayer-like and bilayer-like band structures. The increased phase coherence length at high hole densities takes our shortest devices into the mesoscopic regime with the appearance of significant conductance fluctuations on top of the localization effects. Although these are aperiodic in gate voltage, they exhibit a quasi-periodic behaviour as a function of magnetic field. We show that this is consistent with the interference of discrete trajectories in open quantum dots and discuss the possible origin of these in our devices.

Keywords: trilayer graphene, weak localization, conductance fluctuations, mesoscopic transport

SQ1 (Some figures may appear in colour only in the online journal)

## 1. Introduction

The study of quantum interference in graphene is a powerful tool to investigate its electronic properties, for example Fabry–Perot quantum interference in suspended graphene has recently revealed a renormalization of the Fermi velocity due to unscreened many-body interactions [1, 2]. The pseudospin quantum number and chirality [3, 4] of charge carriers have been shown to lead to significant deviations from the usual quantum corrections to the classical conductivity in 2D systems [5]. Most striking is the fact that quantum corrections in graphene depend not only on inelastic phase-breaking scattering but also on several distinct elastic scattering mechanisms. The extra layer in bilayer graphene changes the chirality and, as a result, the quantum corrections. Comparisons between the corrections in monolayer and bilayer have highlighted the subtle interplay that exists between competing transport mechanisms [6]. The properties of carriers in few-layer graphene also depend strongly on the number of layers, for example bilayer graphene exhibits a gate tuneable band-gap and trilayer graphene exhibits a gate tuneable band overlap [7, 8], yet how the quantum corrections evolve as the layer number increases is currently not understood.

Trilayer graphene with ABA Bernal stacking or rhombohedral ABC stacking in the absence of a symmetry breaking perpendicular electric field have gapless dispersions around the chemical potential. For ABA stacking the low energy electronic structure of trilayer graphene consists of overlapping linear and quadratic bands. For ABC stacking one finds an approximately cubic dispersion, with the conduction and valence bands touching at a point close to the high symmetry K and K′ points [9]. Trilayer graphene with Bernal (ABA) stacking is a key system to investigate in order to bridge the gap between the well-studied mono- and bi-layer graphene systems and the complex, little studied multi-layer ones. This is because the low energy band structure of charge carriers is composed of monolayer-like and bilayer-like parts. As a result, it is expected that quantum corrections in this system can be described by a combination of the corrections arising from the two components [10]. Here we describe systematic investigations of weak localization (WL) and conductance fluctuations (CFs) as a function of gate voltage, magnetic field and temperature in short (of the same order of

 

magnitude as the carrier phase-breaking length) channels in a trilayer graphene FET.

The constructive interference of an electron circumscribing time-reversed paths along a closed loop is the origin of the WL correction to the classical Drude conductivity in 2D systems. At the point of intersection, the interference will be constructive if the phase change of the waves is the same along the two paths. Consequently, the probability of the electron remaining at the intersection increases resulting in an increase of the overall electrical resistance. Magnetic flux that threads such a loop adds a random relative phase to the electron waves, which destroys the time reversal symmetry. The charge carriers in monolayer graphene are chiral and their wavefunctions have an associated Berry phase of $\pi$ [11]. Therefore, a closed trajectory will produce a phase difference of $\pi/2$ at the intercept and weak anti-localization (WAL) occurs. However, under most experimental conditions, WL is observed instead [5]. This is a result of two competing elastic scattering mechanisms that occur within (intra-valley) and between (inter-valley) the two Dirac cones. Intra-valley scattering breaks pseudospin conservation and suppresses localization; inter-valley scattering effectively mixes the two cones (that have mirrored chirality) and enhances localization. In bilayer graphene, the Berry phase is $2\pi$ so WL is expected, even in the absence of elastic [10, 12, 13] scattering. Such scattering has the same effect in bilayer graphene as it does in monolayer so no transition to WAL is possible.

In the mesoscopic regime $\left(L \sim L_{\varphi}\right)$, electrons that scatter between two points along all coherent paths have a random phase at the meeting point. As a result, the conductance of a sample in this regime has a random quantum correction that can be changed by moving the scattering centres, applying a perpendicular magnetic field or changing the Fermi energy [14, 15]. For a diffusive system $\left(k_F l \gg 1\right)$, where $l$ is the carrier mean free path, the standard deviation of these random fluctuations is universal, being of the order of $e^2/h$. Such universal CFs have been observed in monolayer [16] and bilayer graphene [10]. Like WL, they are affected by elastic intra- and inter-valley scattering though in a rather more complex way [17]. For a ballistic open quantum dot, a quasi-periodic dependence of the fluctuations on magnetic field can result from the finite size of the system [18].

## 2. Sample fabrication and characterization

Four-terminal field-effect devices were created by micromechanical cleavage of natural graphite (NGS Naturgraphit GmbH, graphenium flakes 1.0–1.8 mm) and deposition onto $Si/SiO_2$ substrates, figures 1(a), (b). Highly doped Si substrates with a 297 nm $SiO_2$ top layer were used as these are known to give good contrast for deposited graphene flakes under an optical microscope [19, 20]. The $SiO_2$ layer also acts as a robust dielectric allowing the highly doped Si substrate to be used as a gate up to relatively high voltages at low temperature $\left(V_g \sim \pm\ 100\ \mathrm{V}\right)$.

The trilayer graphene flake investigated here has been characterized by both atomic force microscopy and Raman spectroscopy in order to establish its quality and layer number, figures 1(c), (d). The height measurement shown in the inset of figure 1(c) results in a thickness of $0.88 \pm 0.17$ nm, which is close to the value expected for trilayer graphene [21]. The Raman spectrum (taken using a 532 nm laser) shows the characteristic G band and 2D band peaks as well as the G* band peak. The D-band peak is absent suggesting that the sample is relatively free of defects [22, 23]. The trilayer nature of the flakes is verified by the need for six Lorentzian components to fully fit the 2D-peak shape [24] as can be seen in the inset of figure 1(d), and an $I(2D)/I(G)$ intensity ratio of 0.4, which is less than 1 expected for bilayer graphene [25, 26].

We have experimented with several different contact metallizations and found that the use of a Pd adhesion layer gave the lowest contact resistances (<100 $\Omega$), presumably due to the fact that Pd is chemisorbed at the graphene surface [27]. Two levels of electron beam lithography have been employed to pattern both the inner electrodes (Pd/Al 10/50 nm) and the outer bond pads (Cr/Au 50/250 nm). The spacings between electrodes varied from 250–750 nm, electrode widths were typically 1.5 $\mu$m and the flake was ~7 m wide. Devices were mounted onto a temperature-controlled sample holder coupled via exchange gas to a liquid helium bath. This system allowed small signal magnetoresistance measurements in a perpendicular magnetic field up to 1 T at temperatures from 2 to 25 K. Four-terminal resistance measurements were made at a constant current of 1 $\mu$A using a low frequency (32 Hz) lock-in amplifier technique. Due to the extreme 28 : 1 aspect ratio of our devices, the resistance of a 250 nm long junction lies in the range 20–90 $\Omega$. Hence the voltage drop across the device at 1 $\mu$A is no more than 100 $\mu$V, equivalent to the thermal energy at ~1 K or less.

## 3. Results

### 3.1. Classical conduction

Figure 2 shows the carrier mobility, $\mu$, as a function of gate voltage, $V_g$, at 4.2 K, estimated from measurements of $R\left(V_g\right)$ using the standard Drude conductivity formula. Carrier density, $n$, was estimated from the capacitive coupling between gate and channel, $n = \alpha\left(V_g - V_D\right)$. Here $V_D$ is the gate voltage at the charge neutrality point and $\alpha = 7.2 \times 10^{10}\ \mathrm{cm^{-2}\ V^{-1}}$ is a characteristic coefficient for our 297 nm $SiO_2$ gate dielectric. Even in the absence of a gate voltage, our sample is very strongly hole-doped due to proximity doping from the Pd/Al contacts. Charge transfer directly under the metal contact locally shifts the position of the chemical potential in our flake. Even outside the contact region this results in bending of the band structure as the position of the chemical potential relaxes back to its undoped level. Indeed, we were unable to reach the charge neutrality point with the maximum positive back gate voltage that could

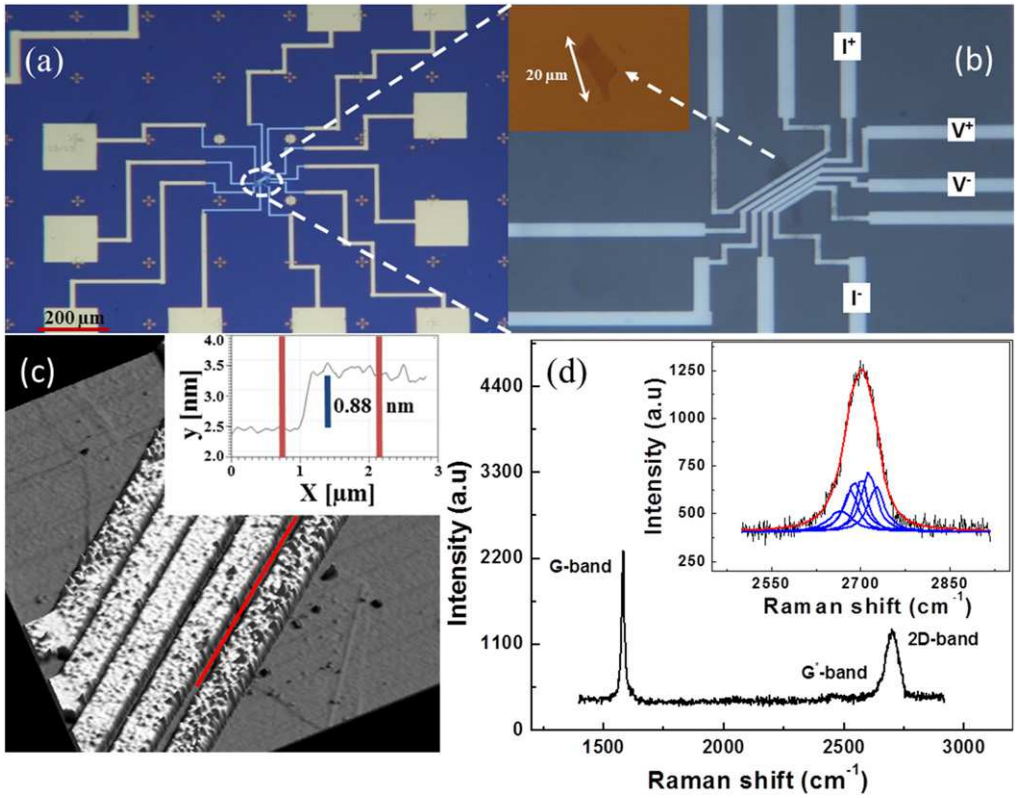


**Figure 1.** (a), (b) Optical micrographs of a trilayer graphene FET at two different magnifications. The inset in (b) shows the trilayer flake after exfoliation. (c) 3D AFM image of the trilayer graphene device. Inset shows the topographic profile of the flake along the line shown. (d) Raman spectrum including expanded view of the 2D-band peak.

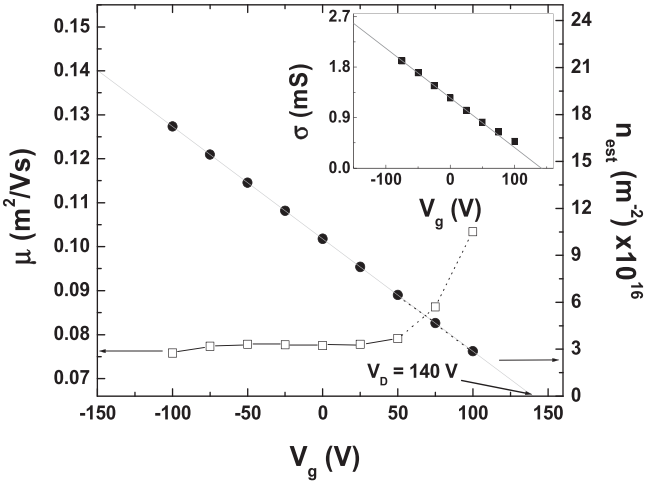


**Figure 2.** Carrier mobility, $\mu$, (open squares) and density, $n$, (filled circles) as a function of gate voltage for the trilayer graphene device at 4.2 K. The inset shows the extrapolation of the conductivity versus gate voltage that was used to estimate the voltage at the charge neutrality point.

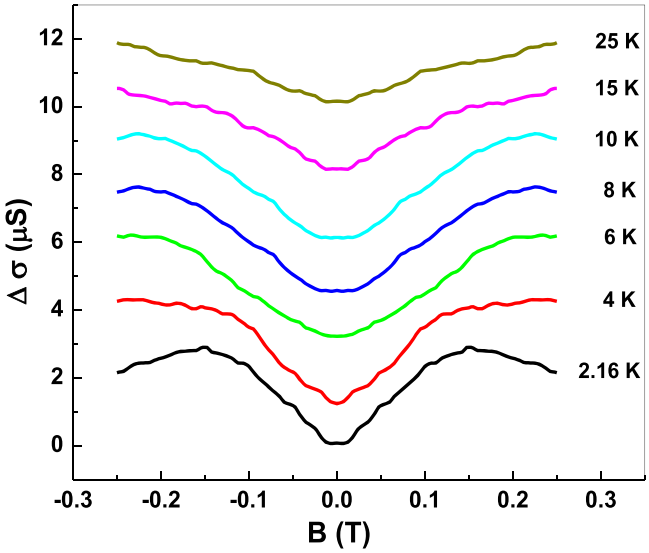


**Figure 3.** Magnetic field dependence of the conductivity as a function of temperature for a 250 nm sample at $V_g = +100$ V. Curves have been offset vertically for clarity.

be applied without dielectric breakdown occurring. However, an extrapolation of the gate voltage-dependent conductivity to zero, figure 2 (inset), allows us to estimate that $V_D = +140 \pm 3$V. From this we calculate the carrier density dependence on gate voltage shown in figure 2. Hole mobilities are found to be in the range 760–1030 $cm^2\,Vs^{-1}$ and lie within the broad range of values obtained for similar devices elsewhere [28–30]. Note that estimates of the mobility near the charge neutrality point are unrealistically high due to the fact that the carrier density theoretically drops to zero there.

### *3.2. The WL correction*

Magnetoconductance data for a 250 nm long trilayer sample at $V_g = +100$ V are shown in figure 3. A very small anti-symmetric component of <5% of $\Delta G$ has been removed from the data by symmetrizing it to facilitate the fitting process. The sharp dip near $B = 0$ at 2.16 K is characteristic of a WL correction and indicates a relatively long phase coherence length at this temperature. With increasing temperature, a pronounced broadening of the WL peak is observed reflecting the reduction of the phase coherence length [16, 31]. For all curves, increasing the applied field from zero leads to a suppression of WL and positive magnetoconductance. However, above a certain field a negative magnetoconductance component is observed, which is more pronounced at low temperatures. This has been observed previously in both epitaxial [32] and exfoliated graphene [5, 10, 33] and is a result of the increasing relative importance of the elastic scattering mechanisms.

To analyse our results, we have used an equation that was derived specifically for graphene [3] and expresses the corrections to the conductance as a function of the inelastic scattering rate $\left(\tau_\varphi^{-1}\right)$ and elastic scattering rates $\left(\tau_i^{-1},\ \tau_*^{-1}\right)$, [31]

$$\frac{\pi h}{e^2}\Delta\sigma(B) = F\left(\frac{\tau_B^{-1}}{\tau_\varphi^{-1}}\right) - F\left(\frac{\tau_B^{-1}}{\tau_\varphi^{-1}+2\tau_i^{-1}}\right) \pm 2F\left(\frac{\tau_B^{-1}}{\tau_\varphi^{-1}+\tau_i^{-1}+\tau_*^{-1}}\right), \quad (1)$$

where $\Delta\sigma(B) = \sigma(B) - \sigma(0)$, $F(z) = \ln z + \psi\left(0.5 + z^{-1}\right)$, $\psi(z)$ is the digamma function, $\tau_B^{-1} = (4eDB)/\hbar$, $\tau_\varphi^{-1}$ is the phase-breaking rate, $\tau_i^{-1}$ is the inter-valley scattering rate and $\tau_*^{-1}$ is the intra-valley scattering rate. The difference between monolayer and bilayer systems is only in the sign of the third term, being negative for monolayer and positive for bilayer. While no specific equation has been derived for trilayer graphene it is expected that it is made up of a combination of those for monolayer and bilayer. As a result, by fitting our data to equation (1) we can investigate the relative monolayer-like and bilayer-like contributions.

The low temperature data for our trilayer graphene device at $V_g = +100$ V could only be fitted by equation (1) if we assumed a negative sign for the third term. This would suggest a domination of the monolayer-like element. Figure 4 shows representative examples of the fits (solid lines) to equation (1) for a 250 nm long sample at three different temperatures. Good agreement is found over the full field range, which allows us to extract values for the dephasing and elastic scattering rates.

The three scattering rates, $\tau_\varphi^{-1}$, $\tau_i^{-1}$ and $\tau_*^{-1}$, extracted from fits to equation (1) are plotted in figure 5. Both $\tau_i^{-1}$ and $\tau_*^{-1}$ have large errors (a result of an interdependence in term 3 of equation (1) and a data set limited by the transport field), but as they are temperature-independent rates the values measured at different temperatures help to reduce this error. We estimate an inter-valley scattering length of $97 \pm 10$ nm, and an intra-valley scattering length of $29 \pm 5$ nm. The latter is rather close to the carrier mean free path ($20 \pm 2$ nm) indicating that the majority of the scattering events that control diffusive transport also contribute to intra-valley scattering.

The dephasing rate varies significantly over the range of temperatures investigated. The approximately linear dependence of $\tau_\varphi^{-1}$ on $T$ is an indication that electron–electron scattering is the dominant phase-breaking mechanism, as seen in monolayer and bilayer systems [32, 34]. The inelastic

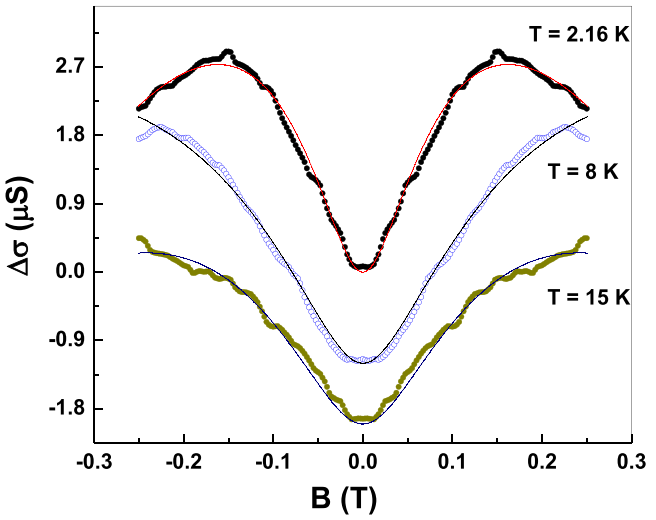


**Figure 4.** Magnetoconductivity of a 250 nm sample at $V_g = +100$ V at three different temperatures. Curves have been offset vertically for clarity. Solid lines are fits to equation (1).

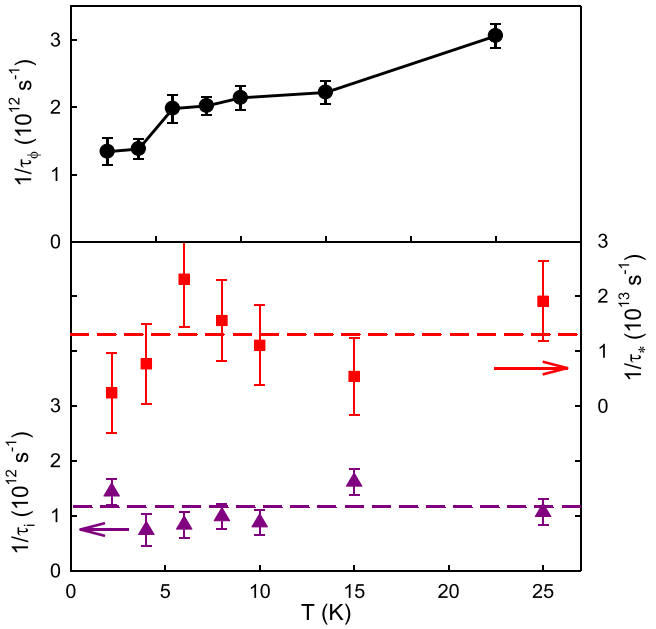


**Figure 5.** Dephasing rate, $\tau_\varphi^{-1}$, and scattering rates $\tau_i^{-1}$ and $\tau_*^{-1}$ as a function of $T$ for a 250 nm long sample at $V_g = +100$ V.

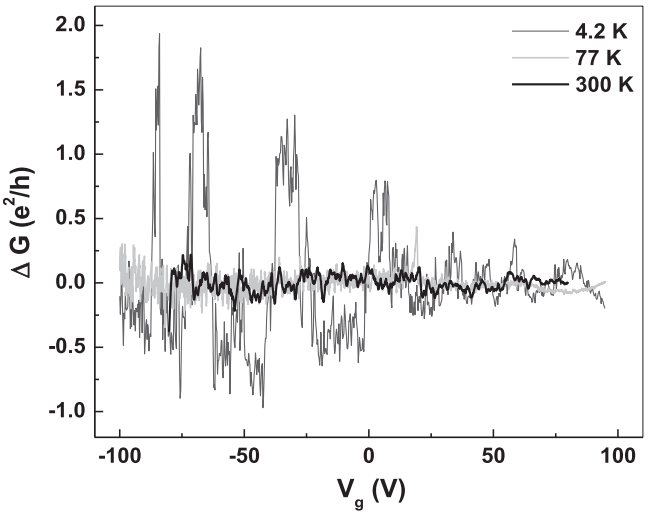


**Figure 6.** $\Delta$G versus $V_g$ for a 250 nm long sample at 4.2 K, 77 K and 300 K. A third order polynomial has been subtracted in each case.

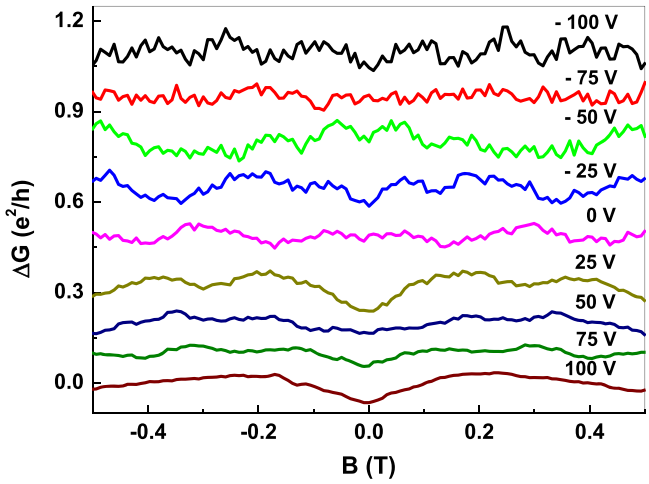


**Figure 7.** $\Delta$G versus $B$ for a 250 nm long channel at various fixed values of $V_g$. A parabolic magnetoresistance background has been subtracted from all curves.

scattering rate at 2.16 K corresponds to a dephasing length of $87 \pm 3$ nm which is several times shorter than the 250 nm length of the channel. This confirms that the sample is not strictly in the mesoscopic limit at $V_g = +100$ V and explains why pronounced CFs are not observed.

### *3.3. CFs*

As our samples become increasingly hole doped at negative gate voltages there is a substantial increase in the dephasing length. Indeed, we estimate that $L_\varphi$ increases from $87 \pm 3$ nm at $V_g = +100$ V to $195 \pm 5$ nm at $V_g = -100\ V$, where it is comparable to the 250 nm channel length of the device. Figure 6 shows the measured conductance as a function of gate voltage in a 250 nm long sample at 300 K, 77 K and 4.2 K. (A third order polynomial has been subtracted from all curves in order to emphasize the CFs.) The 4.2 K data show strong aperiodic CFs with a magnitude of the order of $e^2/h$ at negative gate voltages that decay in amplitude towards the charge neutrality point. This is primarily due to the reduction in the dephasing length as the Dirac point is approached, moving our sample out of the mesoscopic limit.

Figure 7 shows the conductance as a function of magnetic field for a 250 nm long sample at 4.2 K and various gate voltages (a parabolic magnetoresistance background has been subtracted in all cases). Recent experiments have shown that the longitudinal magneto-resistance can be understood as the sum of a Drude term plus a correction due to electron–electron interactions. We find a rather strong temperature-dependence for the concavity of $\rho_{xx}(B)$ in our devices suggesting that the latter may be dominating in our system [35]. At more negative gate voltages, a complex evolution of the magnetoconductance is observed, with strong, quasi-periodic oscillations as a function of magnetic field. This is a clear indication that the device is entering the mesoscopic regime.

A fast Fourier transform of the data has been performed to further analyse the observed periodicity as a function of magnetic field. Figure 8 shows the power spectrum, $F_n$, of the

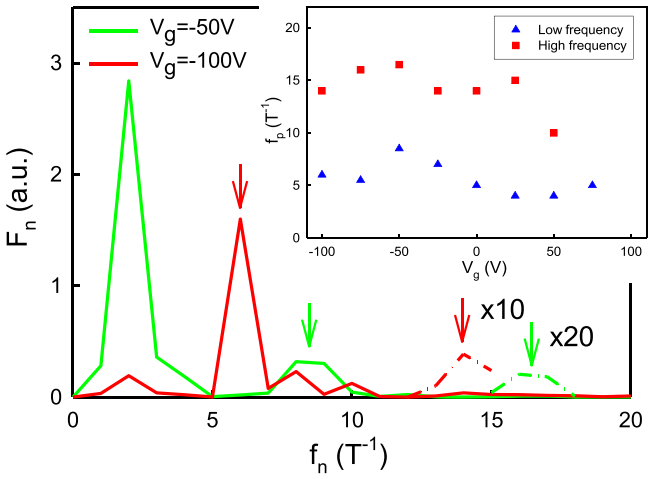


**Figure 8.** FFT analysis of the CFs observed in the conductance of a 250 nm channel at 4.2 K. The power, $F_n$, is plotted as a function of Fourier frequency, $f_n = n/N\delta B$, at two different gate voltages. The two dominant frequencies are indicated by vertical arrows and these are plotted as a function of gate voltage in the inset.

Fourier component at frequency, $f_n = 2\pi n/N\delta B$, for a 250 nm long sample at $V_g = -100$ V and $V_g = -50$ V. Here $N$ is the number of points in a dataset and $\delta B$ the magnetic field spacing between them. Discounting the peak at $n = 2$, which is an artefact of the background subtraction algorithm used, we identify one strong peak in the range $f_1 \sim 4$–$8.5\ \mathrm{T}^{-1}$ at nearly all gate voltages, and in most traces a second, much weaker peak at $f_2 \sim 10$–$15\ \mathrm{T}^{-1}$. This periodic behaviour with a small number of dominant frequency components, as opposed to the aperiodic behaviour normally associated with universal CFs, has been observed previously in bilayer graphene systems [36] and is well-known in the case of open semiconductor-based quantum dots [37]. Assuming this to be a suitable model we can analyse these oscillations in terms of the interference of one or two discrete orbits and estimate the area enclosed by a given orbit from the Aharonov–Bohm

criterion, $A = \left(f_n \cdot h\right)/e$. This yields areas of ~0.017–0.035 $\mu m^2$ and ~0.041–0.062 $\mu m^2$ for the long and short periods, respectively. These correspond to effective circular dots with diameters ~150–210 nm and ~230–280 nm, which are comparable to the 250 nm length of the channel.

The origin of open dots in our samples is likely to be related to the interface between graphene and the Pd/Al contacts. We have already noted that the Pd leads to very strong proximity hole doping in our sample due to the large work function difference. This implies that there must be strong band bending across the active channel region of our devices which, in the case of homogenous contact metallization, would lead to a form of 1D quantum well across the device. However, spatial inhomogeneity of the contacts and/or additional disorder due to trapped charges in the gate dielectric layer will readily break this symmetry and form local dot-like regions. Both the dot size and the gate voltage represent control parameters for the observed dominant CF frequencies [38]. The most likely reason for the presence of two dominant frequencies in our CF data is that they arise from two differently sized open quantum dots, one of which has much lower transmission probability than the other. However, it is also possible that both oscillations arise from the same quantum dot but are associated with the monolayer graphene-like and bilayer graphene-like dispersions.

## 4. Discussion

The periodic CFs observed as a function of magnetic field are consistent with a picture of interfering discrete trajectories around the perimeter of open quantum dots. Since the effective diameter of these is estimated to be close to the channel length of our devices it is likely that they are bounded by the interfacial regions between the graphene and the Pd/Al contacts. It is well established that the large work function difference between Pd and graphene leads to carrier injection and strong hole doping in the graphene. This has been investigated theoretically with a view to optimizing contact resistances to graphene by highly doping the contact region [39, 40]. Using density functional theory calculations of graphene on different metal substrates, Giovannetti *et al* [27]. Developed a phenomenological model that predicts the shift in $E_F$ of graphene when in contact with a number of metals. However, the chemisorption of Pd is particularly strong because of hybridization between the graphene $p_z$ orbitals and the metal d-orbitals, heavily distorting the graphene bands [41]. A charge-transfer model was introduced by Nouchi *et al* [42] to describe the doping effect of metal contacts in the adjacent graphene sheet. These authors introduced a characteristic length, $L_d$, over which the graphene is doped by the metal contact which is typically of the order of 1 $\mu$m. Since this length is substantially larger than the channel length of our smallest devices, and the proximity doping profiles of two adjacent Pd/Al contacts will strongly overlap, one would expect the band bending along the channel to exhibit a fairly shallow minimum. Nouchi *et al* [42] consider two different possible piecewise-linear doping profiles. The first assumes that the charge density is pinned at the metal contacts for all gate voltages while the second represents the case where the charge density is unpinned at the metal contacts and free to vary with gate voltage. As a consequence band bending in the channel can be compensated at an appropriate gate voltage in the pinned model, while it is essentially independent of gate voltage in the unpinned model. In our experiments, we observe $B$-periodic CFs with approximately the same field period at all gate voltages studied, suggesting that the unpinned model appears more appropriate. However, these considerations overlook the additional doping caused by molecular adsorption on the graphene surface and/or ionized charge traps in the $Si/SiO_2$ substrate, as well as possible inhomogeneity of the metal/graphene contacts. It seems likely that these additional phenomena would break the 1D symmetry of the proximity doping profile, leading to the formation of one or more open quantum dots within the channel. Hence a much more detailed analysis of the data would be required to clearly distinguish between pinned and unpinned charge density models.

There are a number of features in our measurements that point to a subtle interplay between transport associated with the monolayer-like and bilayer-like bands present in trilayer graphene. Close to the charge neutrality point, where CFs are suppressed due to a relatively short dephasing length, the localization corrections to the classical conductivity are well described by the form of equation (1) for monolayer graphene. Indeed the bilayer form of the theory does not even provide a qualitative description of the data suggesting that these quantum corrections arise in the monolayer-like band in this regime. An increase in hole density at more negative gate voltages is accompanied by a strong increase in the dephasing length, and the data become complicated by the presence of additional CFs in the mesoscopic limit. Nevertheless, it can be seen from figure 7 that the amplitude of the characteristic WL minimum near $B = 0$ appears to oscillate with gate voltage suggesting a complex competition as a function of $V_g$ between signals arising from the two dispersions.

## 5. Conclusions

We have systematically studied the quantum transport in short trilayer-graphene field-effect transistors. Near the charge neutrality point, when the dephasing length is several times smaller than the channel length, we observe clear WL corrections to the classical conductivity which are well described by the theory developed for monolayer graphene. However, as the hole density and dephasing length increase at more negative gate voltages we see a complex evolution of the conductance minimum near $B = 0$. This suggests a subtle interplay between the contributions of the monolayer graphene-like and bilayer graphene-like bands to these quantum corrections in trilayer graphene. At high hole densities the dephasing length becomes comparable to the length of the channel of the shortest devices. In this limit, we see strong

CFs with amplitude ~$e^2/h$ which are aperiodic in gate voltage. The dominant fluctuations are quasi-periodic in magnetic field with two dominant magnetic frequencies. We interpret this in terms of the interference of discrete carrier trajectories around the perimeter of open quantum dots created by band bending induced at the interface between the graphene and Pd contacts.

## Acknowledgements

We acknowledge valuable discussions with Edward McCann Q2 and Marcin Mucha-Kruczynski. This work was supported financially by the Egyptian government and Ain Shams University, the Engineering and Physical Sciences Research Council (EPSRC) in the UK under grant nos. EP/G036101/1 and the NanoSC COST Action MP-1201.

## Q3 References

[1] Oksanen M, Uppstu A, Laitinen A, Cox D J, Craciun M F, Russo S, Harju A and Hakonen P 2014 *Phys. Rev.* B **89** 121414
[2] Kotov V N, Uchoa B, Pereira V M, Guinea F and Neto A C 2012 *Rev. Mod. Phys.* **84** 1067
[3] McCann E, Kechedzhi K, Fal'ko V I, Suzuura H, Ando T and Altshuler B 2006 *Phys. Rev. Lett.* **97** 146805
[4] Morpurgo A F and Guinea F 2006 *Phys. Rev. Lett.* **97** 196804
[5] Tikhonenko F V, Kozikov A A, Savchenko A K and Gorbachev R V 2009 *Phys. Rev. Lett.* **103** 226801
[6] Horsell D, Tikhonenko F, Gorbachev R and Savchenko A 2008 *Phil. Trans. R. Soc.* A **366** 245–50
[7] Craciun M, Russo S, Yamamoto M, Oostinga J B, Morpurgo A and Tarucha S 2009 *Nat. Nanotechnology* **4** 383–8
[8] Craciun M, Russo S, Yamamoto M and Tarucha S 2011 *Nano Today* **6** 42–60
[9] Aoki M and Amawashi H 2007 *Solid State Commun.* **142** 123–7
[10] Staley N E, Puls C P and Liu Y 2008 *Phys. Rev.*B **77** 155429
[11] Novoselov K S, Geim A K, Morozov S V, Jiang D, Katsnelson M I, Grigorieva I V, Dubonos S V and Firsov A A 2005 *Nature* **438** 197–200
[12] Kechedzhi K, Fal'ko V I, McCann E and Altshuler B 2007 *Phys. Rev. Lett.* **98** 176806
[13] Gorbachev R, Tikhonenko F, Mayorov A, Horsell D and Savchenko A 2007 *Phys. Rev. Lett.* **98** 176805
[14] Altshuler B 1985 *JETP Lett.* **41** 648–51
[15] Lee P A and Stone A D 1985 *Phys. Rev. Lett.* **55** 1622
[16] Chen Y-F, Bae M-H, Chialvo C, Dirks T, Bezryadin A and Mason N 2010 *J. Phys.: Condens. Matter.* **22** 205301
[17] Horsell D, Savchenko A, Tikhonenko F, Kechedzhi K, Lerner I and Fal'ko V 2009 *Solid State Commun.* **149** 1041–5
[18] Bøggild P, Kristensen A, Bruus H, Reimann S M and Lindelof P E 1998 *Phys. Rev.*B **57** 15408
[19] Abergel D, Russell A and Falko V I 2007 *Appl. Phys. Lett.* **91** 063125–3
[20] Blake P, Hill E, Castro Neto A, Novoselov K, Jiang D, Yang R, Booth T and Geim A 2007 *Appl. Phys. Lett.* **91** 063124–3
[21] Nemes-Incze P, Osváth Z, Kamarás K and Biró L 2008 *Carbon* **46** 1435–42
[22] Ferrari A, Meyer J, Scardaci V, Casiraghi C, Lazzeri M, Mauri F, Piscanec S, Jiang D, Novoselov K and Roth S 2006 *Phys. Rev. Lett.* **97** 187401
[23] Malard L, Pimenta M, Dresselhaus G and Dresselhaus M 2009 *Phys. Rep.* **473** 51–87
[24] Cong C, Yu T, Sato K, Shang J, Saito R, Dresselhaus G F and Dresselhaus M S 2011 *ACS Nano* **5** 8760–8
[25] Graf D, Molitor F, Ensslin K, Stampfer C, Jungen A, Hierold C and Wirtz L 2007 *Nano Lett.* **7** 238–42
[26] Gupta A, Chen G, Joshi P, Tadigadapa S and Eklund P 2006 *Nano Lett.* **6** 2667–73
[27] Giovannetti G, Khomyakov P, Brocks G, Karpan V, Van den Brink J and Kelly P 2008 *Phys. Rev. Lett.* **101** 026803
[28] Geim A K and Novoselov K S 2007 *Nat. Mater.* **6** 183–91
[29] Novoselov K S, Geim A K, Morozov S V, Jiang D, Zhang Y, Dubonos S V, Grigorieva I V and Firsov A A 2004 *Science* **306** 666–9
[30] Tan Y W, Zhang Y, Stormer H L and Kim P 2007 *Eur. Phys. J.-Spec. Top.* **148** 15–8
[31] Tikhonenko F, Horsell D, Gorbachev R and Savchenko A 2008 *Phys. Rev. Lett.* **100** 56802
[32] Wu X, Li X, Song Z, Berger C and De Heer W A 2007 *Phys. Rev. Lett.* **98** 136801
[33] SiangáLew W 2011 *Phys. Chem. Chem. Phys.* **13** 20208–14
[34] Berger C, Song Z, Li X, Wu X, Brown N, Naud C, Mayou D, Li T, Hass J and Marchenkov A N 2006 *Science* **312** 1191–6
[35] Jobst J, Waldmann D, Gornyi I V, Mirlin A D and Weber H B 2012 *Phys. Rev. Lett.* **108** 106601
[36] Ujiie Y, Motooka S, Morimoto T, Aoki N, Ferry D, Bird J and Ochiai Y 2009 *J. Phys. Condens. Matter.* **21** 382202
[37] Bird J, Akis R, Ferry D, de Moura A, Lai Y and Indlekofer K 2003 *Rep. Prog. Phys.* **66** 583
[38] Ferry D, Burke A, Akis R, Brunner R, Day T, Meisels R, Kuchar F, Bird J and Bennett B 2011 *Semicond. Sci. Technol.* **26** 043001
[39] Nagashio K, Nishimura T, Kita K and Toriumi A 2009 *Electron Devices Meeting (IEDM), 2009 IEEE Int.* (IEEE) pp 1–4
[40] Nagashio K, Nishimura T, Kita K and Toriumi A 2010 *Appl. Phys. Lett.* **97** 143514
[41] Khomyakov P, Giovannetti G, Rusu P, Brocks G, Van den Brink J and Kelly P 2009 *Phys. Rev.* B **79** 195425
[42] Nouchi R and Tanigaki K 2010 *Appl. Phys. Lett.* **96** 253503